

Exact new mobility edges between critical and localized states

Xin-Chi Zhou,^{1,2,*} Yongjian Wang,^{3,4,*} Ting-Fung Jeffrey Poon,^{1,2,*} Qi Zhou,^{5,†} and Xiong-Jun Liu^{1,2,6,‡}

¹International Center for Quantum Materials, School of Physics, Peking University, Beijing 100871, China

²Hefei National Laboratory, Hefei 230088, China

³School of Mathematics and Statistics, Nanjing University of Science and Technology, Nanjing 210094, China

⁴School of Mathematical Sciences, Laboratory of Mathematics and Complex Systems, MOE, Beijing Normal University, Beijing 100875, China

⁵Chern Institute of Mathematics and LPMC, Nankai University, Tianjin 300071, China

⁶International Quantum Academy, Shenzhen 518048, China

The disorder systems host three types of fundamental quantum states, known as the extended, localized, and critical states, of which the critical states remain being much less explored. Here we propose a class of exactly solvable models which host a novel type of exact mobility edges (MEs) separating localized states from robust critical states, and propose experimental realization. Here the robustness refers to the stability against both single-particle perturbation and interactions in the few-body regime. The exactly solvable one-dimensional models are featured by quasiperiodic mosaic type of both hopping terms and on-site potentials. The analytic results enable us to *unambiguously* obtain the critical states which otherwise require arduous numerical verification including the careful finite size scalings. The critical states and new MEs are shown to be robust, illustrating a generic mechanism unveiled here that the critical states are protected by zeros of quasiperiodic hopping terms in the thermodynamic limit. Further, we propose a novel experimental scheme to realize the exactly solvable model and the new MEs in an incommensurate Rydberg Raman superarray. This work may pave a way to precisely explore the critical states and new ME physics with experimental feasibility.

Introduction.—Anderson localization (AL) is a fundamental and ubiquitous quantum phenomenon that quantum states are exponentially localized due to disorder [1]. Scaling theory shows that all noninteracting states are localized in one and two dimensions with arbitrarily small disorder strength [2, 3], while in three dimension (3D), the localized and extended states can coexist at finite disorder strength, and be separated by a critical energy E_c , dubbed the mobility edge (ME). The ME leads to various fundamental phenomena, such as metal-insulator transition by varying the particle number density or disorder strength [4]. Moreover, a system with ME exhibits strong thermoelectric response, enabling application in thermoelectric devices [5–7]. An important feature of ME between extended and localized states is that it is stable, and can survive under perturbations and interactions [8–12].

Unlike in randomly disordered system, the extended-AL transition and ME can exist in 1D system with quasiperiodic potential [13–30]. This result has triggered lots of experimental studies in realizing quasiperiodic systems with ultracold atoms [31–41] and other systems like photonic crystals, optical cavities, and superconducting circuits [42–47]. More importantly, quasiperiodic systems can host a third type of states called critical states [47–52]. The critical states are extended but non-ergodic, locally scale-invariant and fundamentally different from the localized and extended states in spectral statistics [53–55], multifractal properties [56–58], and dynamical evolution [59–61]. With interactions, the single-particle critical states may become many-body critical (MBC) phase [29, 62, 63] that interpolates the thermal and many-body localized phase [64, 65]. However, unlike localized and extended states, to confirm critical states is more subtle and requires arduous numerical calculations like finite-size scaling. It remains unclear what generic mechanism leads to the critical states. Therefore, it is highly important to develop

exactly solvable models with critical states being unambiguously determined and fully characterized. Moreover, similar to the ME for extended and localized states, are there new MEs separating critical from localized states [25], in particular, in experimentally feasible models? A definite answer to this fundamental question is yet elusive but may be provided by resolving the following issues. First, one can develop exactly solvable models with analytic MEs between critical and localized states. Further, one needs to confirm that such new MEs are robust, e.g. in the presence of perturbation and/or interactions. Finally, the proposed exactly solvable models are feasible in experimental realization.

In this Letter, we propose a class of exactly solvable 1D models featured with mosaic type quasiperiodic hopping coefficients and on-site potential, and obtain *unambiguously* critical states and robust exact MEs. The new MEs fundamentally distinct from those in previous exact solvable models [23]. The localization and critical features of all quantum states in the spectra are precisely determined by extending Avila’s global theory [66], enabling an accurate characterization of the critical states and new MEs. We further confirm the robustness of MEs against single-particle perturbation and interactions in the few-body regime. The robustness is rooted in a profound mechanism unveiled with our exactly solvable models that the critical states are protected by incommensurately distributed zeros of mosaic hopping terms in thermodynamic limit. Finally, we propose a novel scheme with experimental feasibility to realize and detect the exact MEs in *Raman superarray* of Rydberg atoms.

Model.—We propose a class of quasiperiodic mosaic models as pictorially shown in Fig. 1(a), and described by

$$H = \sum_j (t_j a_j^\dagger a_{j+1} + \text{h.c.}) + \sum_j V_j n_j, \quad (1)$$

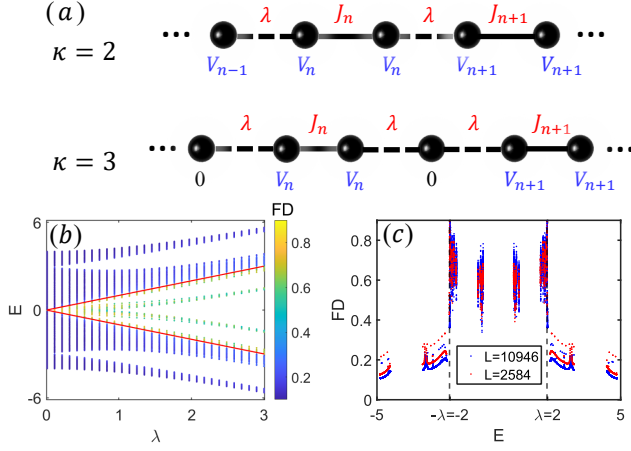


Figure 1. (a) The 1D quasiperiodic mosaic model with $\kappa = 2$ and $\kappa = 3$. The black solid and dashed lines denote the quasiperiodic hopping ($t_j = J_n$) and constant hopping ($t_j = \lambda$), respectively. The black sphere denotes a lattice site, and V_n is the quasiperiodic mosaic potential. Here $J_n = V_n = 2t_0 \cos(2\pi\kappa\alpha n)$, n is an integer. (b) Fractal dimension (FD) of different eigenstates as a function of corresponding energies E and λ for $L = 2584$. The red lines denote the MEs $E_c = \pm\lambda$. (c) FD versus E with fixed $\lambda = 2.0$ for $L = 2584$ (red dots) and $L = 10946$ (blue dots). The dashed lines represent the MEs. The t_0 is set to 1 as energy unit.

where the particle number operator $n_j = a_j^\dagger a_j$, with a_j^\dagger (a_j) the creation (annihilation) operator at site j , and the key ingredients in the models are that both the quasiperiodic hopping coefficient t_j and on-site potential V_j are mosaic, with

$$\{t_j, V_j\} = \begin{cases} \{\lambda, 2t_0 \cos[2\pi\alpha(j-1) + \theta]\}, & j = 1 \bmod \kappa, \\ 2t_0 \cos(2\pi\alpha j + \theta)\{1, 1\}, & j = 0 \bmod \kappa, \\ \{\lambda, 0\}, & \text{else.} \end{cases} \quad (2)$$

Here κ is an integer and $\kappa \geq 2$. λ and θ denote hopping coefficient and phase offset, respectively. We take for convenience $t_0 = 1$, and set $\theta = 0$ and $\alpha = \lim_{n \rightarrow \infty} (F_{n-1}/F_n) = (\sqrt{5} - 1)/2$ without affecting generality, with F_n being Fibonacci numbers. For finite system one may choose the system size $L = F_n$ and $\alpha = F_{n-1}/F_n$ to impose the periodic boundary condition for numerical diagonalization of the tight-binding model in Eq. (1). To facilitate our discussion we focus on the minimal model for $\kappa = 2$ in main text. The results with $\kappa > 2$ are put in Supplemental Material [67]. We shall prove that the minimal model has exact energy-dependent MEs separating localized states and critical states, which are given by

$$E_c = \pm\lambda. \quad (3)$$

Before showing the rigorous proof, we present numerical verification. For this exactly solvable model, the different types of states can be identified by the fractal dimension (FD), defined for an arbitrary m -th eigenstate $|\psi_m\rangle = \sum_{j=1}^L u_{m,j} a_j^\dagger |vac\rangle$ as $FD = -\lim_{L \rightarrow \infty} \ln(IPR)/\ln(L)$, with the inverse participation ratio (IPR) being $IPR = \sum_j |u_{m,j}|^4$. The FD tends

to 1 and 0 for the extended and localized states, respectively, while $0 < FD < 1$ for critical states. Fig. 1(b) shows FD as a function of λ for different eigenstates of eigenvalues E . The red lines starting from band center denote the MEs $E_c = \pm\lambda$, across which FD changes from values close to 0.5 to values close to 0, indicating a critical-to-localization transition predicted by the analytic results. Particularly, we fix $\lambda = 2.0$ and show FD of different eigenstates in Fig. 1(c) as a function of the corresponding eigenvalues for different sizes. The dashed lines in the figure are the MEs $E_c = \pm\lambda = \pm 2.0$. One can observe that the fractal dimension FD tends to 0 for all states in energy zones with $|E| > \lambda$ with increasing the system size, implying that those states are localized. On the contrast, in energy zones with $|E| < \lambda$, the FD magnitude is far different from 0 and 1, and nearly independent of the system size. A more careful finite size scaling for FD can be found in [67].

Rigorous proof.—The MEs of the models in Eqs. (1)-(2) can be analytically obtained by computing Lyapunov exponent (LE) γ_ϵ in combination with zeros of hopping coefficients, which provides the unambiguous evidence of the critical zone. Denote T_i to be the one-step transfer matrix of the Schrödinger operator at site i , i.e. $(C_{i+1}, C_i)^\top = T_i(C_i, C_{i-1})^\top$ and $\mathcal{T}_i = T_i T_{i-1} \cdots T_1$. The LE γ_0 for a state with energy E is computed via $\gamma_\epsilon(E) = \lim_{m \rightarrow \infty} \int d\theta \ln \|\mathcal{T}_m(\theta + i\epsilon)\| / (2\pi m)$, where $\|\cdot\|$ denotes the norm of matrix and ϵ is imaginary part of complexified θ . We will extend Avila's global theory [66] to singular cocycles, and show that $\gamma_0 = \lim_{\epsilon \rightarrow \infty} \gamma_\epsilon = \kappa^{-1} \ln \|\lim_{\epsilon \rightarrow \infty} \mathcal{T}_\kappa(\theta + i\epsilon)\|$ [68]. In particular for $\kappa = 2$,

$$\mathcal{T}_2(\theta + i\epsilon) = \frac{1}{\lambda M} \begin{pmatrix} E - M & -M \\ \lambda & 0 \end{pmatrix} \begin{pmatrix} E - M & -\lambda \\ M & 0 \end{pmatrix},$$

where $M = 2 \cos(2\pi\alpha + \theta + i\epsilon)$ so that the LE is given by

$$\gamma_0(E) = \frac{1}{2} \ln \left| |E/\lambda| + \sqrt{(E/\lambda)^2 - 1} \right|. \quad (4)$$

For $|E| > |\lambda|$, one has $\gamma_0(E) > 0$ and the state associated with E is localized with the localization length $\xi(E) = \gamma_0^{-1}$. If $|E| < |\lambda|$, $\gamma_0(E) = 0$ and for such LE the eigenstates can in general be either extended or critical, which belong to absolutely continuous (AC) spectrum or singular continuous (SC) spectrum, respectively [69]. There are two basic approaches to rule out the existence of AC spectrum (extended states), one is introducing unbounded spectrum [25] and the other is introducing zeros of hopping terms in Hamiltonian [70, 71]. For our model, there exists a sequence of sites $\{2j_k\}$ such that $t_{2j_k} \rightarrow 0$ in the thermodynamics limit, so there is no AC spectrum (extended states) [72], and the eigenstates associated with $|E| \leq |\lambda|$ are all critical. In summary, vanishing LEs $\gamma_0 = 0$ and zeros of incommensurate hopping coefficients altogether unambiguously determine the critical region for $|E| \leq |\lambda|$ and positive LEs determine the localized region for $|E| > |\lambda|$. Therefore $E = \pm\lambda$ mark critical energies separating localized states and critical states, manifesting MEs.

Mechanism of critical states.—The emergence of MEs and critical states has a universal underlying mechanism unveiled

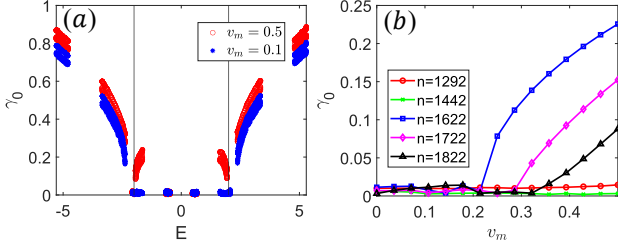


Figure 2. Numerical LEs γ_0 for perturbation strength v_m . (a) γ_0 as a function of eigenvalues E for different v_m . Solid lines are original MEs. (b) γ_0 as a function of v_m for eigenstates $|\psi_n\rangle$ from the band center ($n = 1292$) to the states nearby original MEs ($n = 1822$). Critical states nearby MEs can be driven to localized states while critical zones nearby band center remains unchanged. The other parameters are $\lambda = 2.0$ and $L = 2584$.

from the exact results. Namely, it is due to incommensurately distributed zeros of hopping coefficients [73] in the thermodynamic limit and vanishing the LE. Such zeros in the hopping coefficient t_j effectively divide system into weakly coupled subchains, ruling out possibility of supporting extended states, and leaving the localized or critical states depending on the corresponding LEs. To further verify there is a plethora of critical states in the whole spectrum, let us consider first the special case with vanishing hopping coefficient $\lambda \rightarrow 0$ [Fig. 1(a)]. In this case the model is divided into a series of dimmers, and each dimer renders a 2×2 matrix with all elements being $J_j = V_j = 2 \cos(2\pi\alpha j)$. Then the eigenvalues are simply $E_1 = 2J_j$ and $E_2 = 0$, of which the former corresponds to the localized states, and the latter represents a zero-energy flat band whose degeneracy equals to half of system size. Note that a linear combination of the zero modes are also eigenstates of the model, which can be either localized, extended or critical. Further inclusion of λ hybridizes the zero-energy flat-band modes and localized modes, yielding the critical states and MEs between them and localized ones. This mechanism also explains emergence of critical states starting from band center. Moreover, the number of critical states equals to that of localized states under the exactly solvable condition, as verified by the numerical counting.

This zero hopping coefficient mechanism also explains a novel feature that the critical zone is robust against single-particle perturbation which tunes the model away from exactly solvable condition. We consider an extra mosaic on-site potential term V_p as perturbation, which represents the mismatch between mosaic hopping and onsite potentials in Hamiltonian given in Eq. (2), and is relevant to real experiment,

$$H_p = H + \sum_j V_j^p n_j, \quad (5)$$

where $V_j^p = v_m \cos(2\pi\alpha j + \theta)$ for even- j sites and $V_j^p = v_m \cos[2\pi\alpha(j-1) + \theta]$ for odd- j sites. Fig. 2 shows numerically calculated LEs for different v_m , with $\lambda = 2$. The sufficiently strong mismatch potentials can drive critical states nearby MEs into localized ones while for critical zones nearby

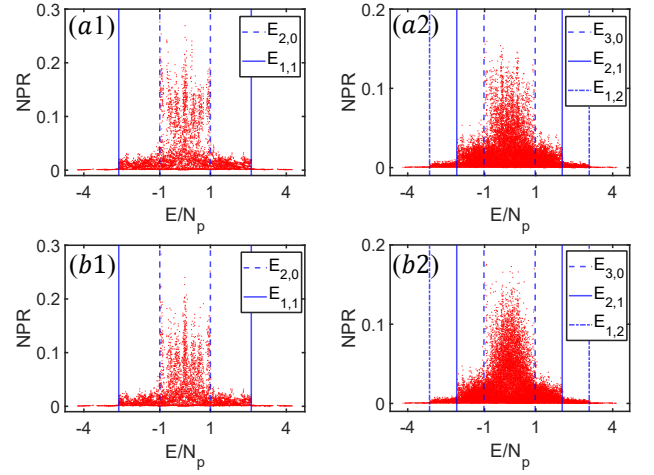


Figure 3. Normalized participation ratio (NPR) as a function of energy density E/N_p of few hardcore bosons with $U = 0$ (upper panel) and $U = 1.4$ (lower panel), with $\lambda = 1.0$ and $t_0 = 1.0$. Critical energy E_{N_c, N_l} is the maximal allowed energy for N_c particles filled in critical orbitals and N_l particles filled in localized orbitals. (a1)(b1) $N_p = 2, L = 120$. (a2)(b2) $N_p = 3, L = 60$. The critical energy $E_{2,0}(E_{3,0})$ is equal to the single particle ME $E = \lambda$ for two(three)-boson case.

the band center the states remains unchanged [Fig. 2(a)]. A more careful investigation of LEs shows that to drive critical states into localized ones requires finite $v_m = v_m^c$, with the magnitude v_m^c depending on the location of the critical state [Fig. 2(b)]. These results manifest the robustness of critical zones against perturbations, which is a key point of the present model. In comparison, the celebrated Aubry-André (AA) model exhibit a self-duality point at $V = 2t$, at which all states are critical [13]. However, those critical states are not robust and shall be quenched to localized state for infinitesimal perturbations. The present study unveils a generic mechanism to obtain robust critical zones protected by the zeros of hopping coefficients with vanishing LEs in the thermodynamic limit, which are not removed by the perturbations. This also shows a nontrivial regime that while Avila's global theory cannot give analytical MEs, the MEs exist.

Robustness against interactions.—We further demonstrate the robustness of MEs in the presence of interactions by studying a few-body Hamiltonian given by

$$H = H_0 + U \sum_j n_j n_{j+1}, \quad (6)$$

where H_0 denotes the system with few hard-core bosons with Hamiltonian in Eq. (1), with $\langle n_j \rangle \leq 1$, and U denotes the strength of neighboring interactions. This model can be simulated with Rydberg atoms (see details in next section). We propose normalized participation ratio (NPR) to detect the MEs in the few-body system. The NPR of an eigenstate $|\psi_m\rangle = \sum_c u_{m,c} |c\rangle$ is defined as $\text{NPR} = 1 / \left(V_H \sum_c |u_{m,c}|^4 \right)$, where $\{c\}$ is the computational basis and V_H is the size of the Hilbert state [74]. When $U = 0$, the

few-body states are product states of single particle orbitals. In the presence of single particle MEs (SPMEs), the few-body states can be categorized into three types [8, 9]: all the particles occupy localized (critical) orbitals, and mixed states with some particles in localized orbitals and others in critical orbitals. Denote the maximum energy of critical (localized) orbitals as λ (E_{\max}), where E_{\max} is the maximum energy of spectrum, we can construct the maximally allowed energy for N_c (N_l) particles filled in critical (localized) orbitals as $E_{N_c, N_l} = (N_c \lambda + N_l E_{\max}) / N_p$ with $N_p = N_c + N_l$. Then E_{N_c, N_l} locates the transition of different types of few-body states, where NPR changes discontinuously. For instance, when $N_p = 3$, the maximal allowed energy for a mixed state with 2 particles filled in critical orbitals and 1 particle filled in localized orbitals is $E_{2,1}$. As shown in Fig. 3(a), NPR displays clear discontinuities at E_{N_c, N_l} as expected.

Our key observation is that the sharp discontinuities near $\pm E_{N_c, N_l}$ persist for $U \neq 0$ for the few-body regime, manifesting the robustness of SPMEs against few-body interactions. As shown in Fig. 3(b), for $U = 1.4$, E_{N_c, N_l} can still identify the NPR transition. This is because only those states with at least two particles occupying neighboring sites can be influenced by the interaction, and the portion of such states is of order $\mathcal{O}(L^{-1})$, with L the system size. Thus for relatively large L almost all eigenstates are still product states of single-particle orbitals, except for the small portion affected by interaction. Note that the localized orbitals have zero contribution to NPR in large L limit, and the number of critical orbitals determine NPR of the few-body states. Thus the NPR exhibits sharp transitions across critical energies of E_{N_c, N_l} , which are related to single particle MEs, showing the robustness of MEs and critical zones in the few-body case. This novel result motivate us to realize the exactly solvable model and observe our predictions with Rydberg atoms arrays [75–77] which are natural platforms to simulate hard-core bosons [78, 79].

Experimental realization.—Finally we propose an experimental scheme dubbed *incommensurate Raman superarray* of Rydberg atoms [Fig. 4(a1,a2)] to realize the model in Eq. (1) with $\kappa = 2$. We see that the realization of the Hamiltonian is precisely mapped to the realization of a two-leg lattice model, with even (odd) sites mapped to the sites on $A(B)$ -leg as pictorially shown in Fig. 4(a2), whose Hamiltonian reads $H = \sum_j (J_j a_j^\dagger b_j + \lambda a_j^\dagger b_{j+1} + \text{H.c.}) + \sum_j V_j (a_j^\dagger a_j + b_j^\dagger b_j)$. This basic idea can be directly generalized to realize models with larger κ by introducing more legs in superarray. The mapped Hamiltonian can be realized by Rydberg atoms based on three key ingredients. (i) The AB-leg superarray has an effective Zeeman splitting gradient applied in the x direction (a2); (ii) two types of nearest neighbour couplings, with constant hopping coupling λ simulated by intrinsic dipole-exchange interaction and quasi-periodic hopping coupling J_j induced by laser-assisted dipolar interaction [80]; and (iii) an on-site incommensurate chemical potential V_j . Two Rydberg states $|\downarrow\rangle = |70, S\rangle \equiv |0\rangle$ and $|\uparrow\rangle = |70, P\rangle \equiv |1\rangle$ are chosen to simulate empty and occupied states at each site. As illustrated in Fig. 4(b1), the intrinsic dipole-dipole interactions be-

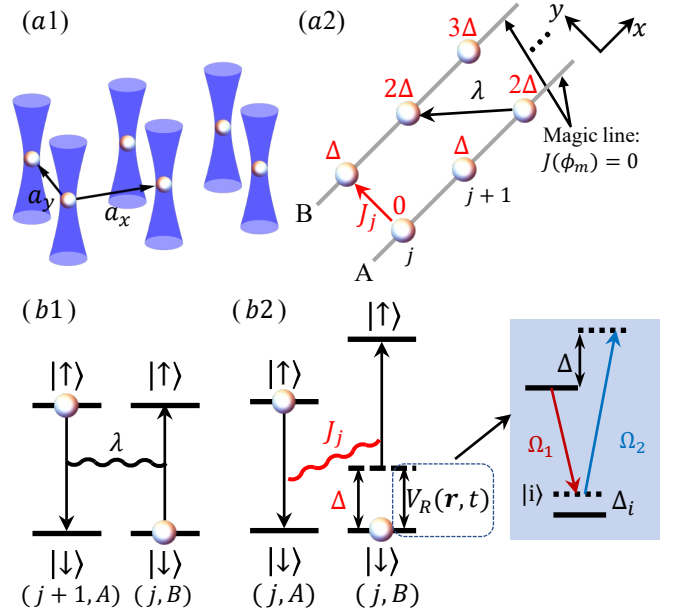


Figure 4. Realization of the quasiperiodic mosaic model with $\kappa = 2$ in incommensurate Raman superarrays of Rydberg atoms. (a1) Rydberg atoms trapped in optical tweezers to form a two-leg array. (a2) The equivalent two-leg lattice model. The incommensurate and constant hopping coefficients are denoted as J_j and λ . An effective Zeeman splitting gradient (red) modifies energy difference between Rydberg states. The Rydberg atoms are trapped along the magic angle ϕ_m , at which the amplitude of dipolar interaction vanishes. (b1) The intrinsic dipole-dipole interaction can induce constant hopping coupling λ . (b2) The inter-leg exchange coupling between A_j and B_j is suppressed by the Zeeman detuning Δ , but can be further restored by applying the Raman coupling potential $V_R \propto \cos(4\pi\alpha j_x) \cos(\pi j_y) e^{i(\omega_2 - \omega_1)t} \sigma_{j_x, j_y}^x + \text{H.c.}$, which is generated by two Raman beams $\Omega_{1,2}$ with frequency difference $\omega_1 - \omega_2 \approx \Delta$ such that the Zeeman splitting can be compensated by two-photon process [Fig. 4(b2)]. Further, the spatial modulation of the Raman potential determines the incommensurate strength of the induced exchange couplings as $J_j = 2t_0 \cos 4\pi\alpha j$ (see Supplemental Material for details [67]). To prohibit laser-assisted exchange couplings along x direction, we use the angular dependence of dipole-dipole interaction $V_{dd} = d^2(1 - 3\cos^2\phi)/R^3$ with d and R being the dipole moment and distance between two Rydberg levels, respectively. There exists a "magic angle" $\phi_m = \arccos(1/\sqrt{3}) \approx 54.7^\circ$ [77, 81], along which the exchange coupling vanishes. By arranging the Rydberg atoms

tween two Rydberg states lead to an exchange coupling, which maps to constant hopping λ of the hard-core bosons [78, 79].

The AB-leg superarray and laser-assisted dipole-dipole interactions altogether realize the incommensurate hopping J_j . The inter-leg exchange couplings between A_j and B_j sites are suppressed by a large energy detuning Δ , but can be further restored by applying the Raman coupling potential $V_R \propto \cos(4\pi\alpha j_x) \cos(\pi j_y) e^{i(\omega_2 - \omega_1)t} \sigma_{j_x, j_y}^x + \text{H.c.}$, which is generated by two Raman beams $\Omega_{1,2}$ with frequency difference $\omega_1 - \omega_2 \approx \Delta$ such that the Zeeman splitting can be compensated by two-photon process [Fig. 4(b2)]. Further, the spatial modulation of the Raman potential determines the incommensurate strength of the induced exchange couplings as $J_j = 2t_0 \cos 4\pi\alpha j$ (see Supplemental Material for details [67]). To prohibit laser-assisted exchange couplings along x direction, we use the angular dependence of dipole-dipole interaction $V_{dd} = d^2(1 - 3\cos^2\phi)/R^3$ with d and R being the dipole moment and distance between two Rydberg levels, respectively. There exists a "magic angle" $\phi_m = \arccos(1/\sqrt{3}) \approx 54.7^\circ$ [77, 81], along which the exchange coupling vanishes. By arranging the Rydberg atoms

along the magic angle, we manage to prohibit coupling in the x direction. Finally, the incommensurate mosaic potential V_j can be realized via AC Stark shift [67]. Adding up those ingredients together we reach the target model. The non-interacting critical states and MEs can be observed from the spectrum when a single hard-core boson is excited in this scheme, while the critical energies depicted in Fig. 3 will be observed when several hard-core bosons are excited in experiment.

Conclusion and discussion.—We have proposed a class of exactly solvable 1D incommensurate mosaic models to realize new and robust MEs separating critical states from localized states, and further proposed a novel experimental realization through incommensurate Raman superarrays of Rydberg atoms. The robust critical states and MEs originate from a combination of zeros of quasiperiodic hopping coefficients in the thermodynamic limit and the zero Lyapunov exponents (LEs), which can be analytically obtained for the proposed models and in agreement with the numerical studies. We note that these two features, serving as a generic mechanism, can provide the guidance to construct broad class of analytic models hosting robust critical states. Moreover, we demonstrate the robustness of MEs and propose NPR as a new probe to detect the MEs in the few-body regime. A future intriguing issue is to explore the interacting effects in the finite filling regime, which might lead to exotic many-body new MEs. Our work broadens the concept of MEs and provides a feasible lattice model that hosts exact MEs and unambiguous critical zones with experimental feasibility.

We thank Yucheng Wang for fruitful discussions. This work was supported by National Key Research and Development Program of China (2021YFA1400900 and 2020YFA0713300), the National Natural Science Foundation of China (Grants No. 11825401, No. 12261160368, No. 12071232, and No. 12061031), and the Innovation Program for Quantum Science and Technology (Grant No. 2021ZD0302000). Q. Zhou was also supported by the Science Fund for Distinguished Young Scholars of Tianjin (No. 19JCJQJC61300) and Nankai Zhide Foundation.

* These authors contribute equally to this work.

† qizhou@nankai.edu.cn

‡ xiongjunliu@pku.edu.cn

- [1] P. W. Anderson, Absence of diffusion in certain random lattices, *Phys. Rev.* **109**, 1492 (1958).
- [2] E. Abrahams, P. W. Anderson, D. C. Licciardello, and T. V. Ramakrishnan, Scaling Theory of Localization: Absence of Quantum Diffusion in Two Dimensions, *Phys. Rev. Lett.* **42**, 673 (1979).
- [3] D. J. Thouless, Electrons in disordered systems and the theory of localization, *Phys. Rep.* **13**, 93 (1974).
- [4] F. Evers and A. D. Mirlin, Anderson transitions, *Rev. Mod. Phys.* **80**, 1355 (2008).
- [5] R. Whitney, Most Efficient Quantum Thermoelectric at Finite Power Output, *Phys. Rev. Lett.* **112**, 130601 (2014).
- [6] C. Chiaracane, M. T. Mitchison, A. Purkayastha, G. Haack, and J. Goold, Quasiperiodic quantum heat engines with a mobility edge, *Phys. Rev. Research* **2**, 013093 (2020).
- [7] K. Yamamoto, A. Aharony, O. Entin-Wohlman, and N. Hatano, Thermoelectricity near Anderson localization transitions, *Phys. Rev. B* **96**, 155201 (2017).
- [8] X. Li, S. Ganeshan, J.H. Pixley, and S. Das Sarma, Many-Body Localization and Quantum Nonergodicity in a Model with a Single-Particle Mobility Edge, *Phys. Rev. Lett.* **115**, 186601 (2015).
- [9] R. Modak and S. Mukerjee, Many-Body Localization in the Presence of a Single-Particle Mobility Edge, *Phys. Rev. Lett.* **115**, 230401 (2015).
- [10] S. Nag and A. Garg, Many-body mobility edges in a one-dimensional system of interacting fermions, *Phys. Rev. B* **96**, 060203(R) (2017).
- [11] F.A. An, K. Padavić, E.J. Meier, S. Hegde, S. Ganeshan, J.H. Pixley, S. Vishveshwara, and B. Gadway, Interactions and Mobility Edges: Observing the Generalized Aubry-André Model, *Phys. Rev. Lett.* **126**, 040603 (2021).
- [12] T. Kohlert, S. Scherg, X. Li, H. P. Lüschen, S. Das Sarma, I. Bloch, and M. Aidelsburger, Observation of Many-Body Localization in a One-Dimensional System with a Single-Particle Mobility Edge, *Phys. Rev. Lett.* **122**, 170403 (2019).
- [13] S. Aubry and G. André, Analyticity breaking and Anderson localization in incommensurate lattices, *Ann. Israel Phys. Soc.* **3**, 133 (1980).
- [14] S. Das Sarma, S. He, and X. C. Xie, Mobility edge in a model one-dimensional potential, *Phys. Rev. Lett.* **61**, 2144 (1988).
- [15] D. J. Boers, B. Goedeke, D. Hinrichs, and M. Holthaus, Mobility edges in bichromatic optical lattices, *Phys. Rev. A* **75**, 063404 (2007).
- [16] J. Biddle, B. Wang, D. J. Priour Jr, and S. Das Sarma, Localization in one-dimensional incommensurate lattices beyond the Aubry-André model, *Phys. Rev. A* **80**, 021603(R) (2009).
- [17] J. Biddle and S. Das Sarma, Predicted mobility edges in one-dimensional incommensurate optical lattices: an exactly solvable model of Anderson localization, *Phys. Rev. Lett.* **104**, 070601 (2010).
- [18] S. Ganeshan, J. H. Pixley, and S. Das Sarma, Nearest neighbor tight binding models with an exact mobility edge in one dimension, *Phys. Rev. Lett.* **114**, 146601 (2015).
- [19] X. Deng, S. Ray, S. Sinha, G. V. Shlyapnikov, and L. Santos, One-dimensional quasicrystals with power-law hopping, *Phys. Rev. Lett.* **123**, 025301 (2019).
- [20] X. Li, X. Li, and S. Das Sarma, Mobility edges in one dimensional bichromatic incommensurate potentials, *Phys. Rev. B* **96**, 085119 (2017).
- [21] H. Yao, H. Khoukli, L. Bresque, and L. Sanchez-Palencia, Critical behavior and fractality in shallow one-dimensional quasiperiodic potentials, *Phys. Rev. Lett.* **123**, 070405 (2019).
- [22] N. Roy and A. Sharma, Fraction of delocalized eigenstates in the long-range Aubry-André-Harper model, *Phys. Rev. B* **103**, 075124 (2021).
- [23] Y. Wang, X. Xia, L. Zhang, H. Yao, S. Chen, J. You, Q. Zhou, and X.-J. Liu, One dimensional quasiperiodic mosaic lattice with exact mobility edges, *Phys. Rev. Lett.* **125**, 196604 (2020).
- [24] S. Roy, T. Mishra, B. Tanatar, and S. Basu, Reentrant Localization Transition in a Quasiperiodic Chain, *Phys. Rev. Lett.* **126**, 106803 (2021).
- [25] T. Liu, X. Xia, S. Longhi, and L. Sanchez-Palencia, Anomalous mobility edges in one-dimensional quasiperiodic models, *SciPost Phys.* **12**, 027 (2022).
- [26] J. Fraxanet, U. Bhattacharya, T. Grass, M. Lewenstein, and A. Dauphin, Localization and multifractal properties of the long-

- range Kitaev chain in the presence of an Aubry-André-Harper modulation, *Phys. Rev. B* **106**, 024204 (2022).
- [27] M. Gonçalves, B. Amorim, E. V. Castro and P. Ribeiro, Hidden dualities in 1D quasiperiodic lattice models, *SciPost Phys.* **13**, 046 (2022).
- [28] M. Gonçalves, B. Amorim, E. V. Castro and P. Ribeiro, Critical phase in a class of 1D quasiperiodic models with exact phase diagram and generalized dualities, [arXiv:2208.07886](https://arxiv.org/abs/2208.07886)
- [29] Y. Wang, L. Zhang, S. Niu, D. Yu, X.-J. Liu, Realization and detection of non-ergodic critical phases in optical Raman lattice, *Phys. Rev. Lett.* **125**, 073204 (2020).
- [30] Y. Wang, L. Zhang, W. Sun, T.-F. J. Poon, X.-J. Liu Quantum phase with coexisting localized, extended, and critical zones, *Phys. Rev. B* **106**, L140203 (2022).
- [31] G. Roati, C. D'Errico, L. Fallani, M. Fattori, C. Fort, M. Zaccanti, G. Modugno, M. Modugno, and M. Inguscio, Anderson localization of a non-interacting Bose-Einstein condensate, *Nature (London)* **453**, 895 (2008).
- [32] L. Fallani, J. E. Lye, V. Guarrera, C. Fort, and M. Inguscio, Ultracold Atoms in a Disordered Crystal of Light: Towards a Bose Glass, *Phys. Rev. Lett.* **98**, 130404 (2007).
- [33] C. D'Errico, E. Lucioni, L. Tanzi, L. Gori, G. Roux, I. P. McCulloch, T. Giamarchi, M. Inguscio, and G. Modugno, Observation of a Disordered Bosonic Insulator from Weak to Strong Interactions, *Phys. Rev. Lett.* **113**, 095301 (2014).
- [34] M. Schreiber, S. S. Hodgman, P. Bordia, H. P. Lüschen, M. H. Fischer, R. Vosk, E. Altman, U. Schneider, and I. Bloch, Observation of many-body localization of interacting fermions in a quasirandom optical lattice, *Science* **349**, 842 (2015).
- [35] P. Bordia, H. P. Lüschen, S. S. Hodgman, M. Schreiber, I. Bloch, and U. Schneider, Coupling Identical One-Dimensional Many-Body Localized Systems, *Phys. Rev. Lett.* **116**, 140401 (2016).
- [36] P. Bordia, H. P. Lüschen, S. Scherg, S. Gopalakrishnan, M. Knap, U. Schneider, and I. Bloch, Probing Slow Relaxation and Many-Body Localization in Two-Dimensional Quasiperiodic Systems, *Phys. Rev. X* **7**, 041047 (2017).
- [37] H. P. Lüschen, P. Bordia, S. Scherg, F. Alet, E. Altman, U. Schneider, and I. Bloch, Observation of Slow Dynamics near the Many-Body Localization Transition in One-Dimensional Quasiperiodic Systems, *Phys. Rev. Lett.* **119**, 260401 (2017).
- [38] H. P. Lüschen, S. Scherg, T. Kohlert, M. Schreiber, P. Bordia, X. Li, S. D. Sarma, and I. Bloch, Single-particle mobility edge in a one-dimensional quasiperiodic optical lattice, *Phys. Rev. Lett.* **120**, 160404 (2018).
- [39] F. A. An, E. J. Meier, and B. Gadway, Engineering a flux-dependent mobility edge in disordered zigzag chains, *Phys. Rev. X* **8**, 031045 (2018).
- [40] F. A. An, K. Padavić, E. J. Meier, S. Hegde, S. Ganeshan, J. H. Pixley, S. Vishveshwara, and B. Gadway, Observation of tunable mobility edges in generalized Aubry-André lattices, *Phys. Rev. Lett.* **126**, 040603 (2021).
- [41] Y. Wang, J.-H. Zhang, Y. Li, J. Wu, W. Liu, F. Mei, Y. Hu, L. Xiao, J. Ma, C. Chin, and S. Jia, Observation of Interaction-Induced Mobility Edge in an Atomic Aubry-André Wire, *Phys. Rev. Lett.* **129**, 103401 (2022).
- [42] Y. Lahini, R. Pugatch, F. Pozzi, M. Sorel, R. Morandotti, N. Davidson, and Y. Silberberg, Observation of a localization transition in quasiperiodic photonic lattices, *Phys. Rev. Lett.* **103**, 013901 (2009).
- [43] R. Merlin, K. Bajema, Roy Clarke, F. -Y. Juang, and P. K. Bhattacharya, Quasiperiodic GaAs-AlAs heterostructures, *Phys. Rev. Lett.* **55**, 1768 (1985).
- [44] D. Tanese, E. Gurevich, F. Baboux, T. Jacqmin, A. Lemaître, E. Galopin, I. Sagnes, A. Amo, J. Bloch, and E. Akkermans, Fractal energy spectrum of a polariton gas in a Fibonacci quasiperiodic potential, *Phys. Rev. Lett.* **112**, 146404 (2014).
- [45] V. Goblot, A. Štrkalj, N. Pernet, J. L. Lado, C. Dorow, A. Lemaître, L. Le Gratiet, A. Harouri, I. Sagnes, S. Ravets, A. Amo, J. Bloch and O. Zilberberg, Emergence of criticality through a cascade of delocalization transitions in quasiperiodic chains, *Nat. Phys.* **16**, 832 (2020).
- [46] P. Roushan, C. Neill, J. Tangpanitanon, V.M. Bastidas, A. Megrant, R. Barends, Y. Chen, Z. Chen, B. Chiaro, A. Dunsworth, A. Fowler, B. Foxen, M. Giustina, E. Jeffrey, J. Kelly, E. Lucero, J. Mutus, M. Neeley, C. Quintana, D. Sank, A. Vainsencher, J. Wenner, T. White, H. Neven, D. G. Angelakis, J. Martinis, Spectroscopic signatures of localization with interacting photons in superconducting qubits, *Science* **358**, 6367 (2017).
- [47] H. Li, Y.-Y. Wang, Y.-H. Shi, K. Huang, X. Song, G.-H. Liang, Z.-Y. Mei, B. Zhou, H. Zhang, J.-C. Zhang, S. Chen, S.-P. Zhao, Y. Tian, Z.-Y. Yang, Z. Xiang, K. Xu, D. Zheng and H. Fan, Observation of critical phase transition in a generalized Aubry-André-Harper model with superconducting circuits, *npj Quantum Information* **9**, 40 (2023).
- [48] Y. Hatsugai and M. Kohmoto, Energy spectrum and the quantum Hall effect on the square lattice with nextnearest-neighbor hopping, *Phys. Rev. B* **42**, 8282 (1990).
- [49] J. H. Han, D. J. Thouless, H. Hiramoto, and M. Kohmoto, Critical and bicritical properties of Harper's equation with next-nearest-neighbor coupling, *Phys. Rev. B* **50**, 11365(1994).
- [50] Y. Takada, K. Ino, and M. Yamanaka, Statistics of spectra for critical quantum chaos in one-dimensional quasiperiodic systems, *Phys. Rev. E* **70**, 066203 (2004).
- [51] F. Liu, S. Ghosh, and Y. D. Chong, Localization and adiabatic pumping in a generalized Aubry-André-Harper model, *Phys. Rev. B* **91**, 014108 (2015).
- [52] J. Wang, X.-J. Liu, X. Gao, and H. Hu, Phase diagram of a non-Abelian Aubry-André-Harper model with p-wave superfluidity, *Phys. Rev. B* **93**, 104504 (2016).
- [53] T. Geisel R. Ketzmerick and G. Petschel, New class of level statistics in quantum systems with unbounded diffusion, *Phys. Rev. Lett.* **66**, 1651 (1991).
- [54] K. Machida and M. Fujita, Quantum energy spectra and one-dimensional quasiperiodic systems, *Phys. Rev. B* **34**, 7367 (1986).
- [55] C. L. Bertrand and A. M. García-García, Anomalous thouless energy and critical statistics on the metallic side of the many-body localization transition, *Phys. Rev. B* **94**, 144201 (2016).
- [56] T. C. Halsey, M. H. Jensen, L. P. Kadanoff, I. Procaccia, and B. I. Shraiman, Fractal measures and their singularities: The characterization of strange sets, *Phys. Rev. A* **33**, 1141 (1986).
- [57] A. D. Mirlin, Y. V. Fyodorov, A. Mildenerger, and F. Evers, Exact Relations Between Multifractal Exponents at the Anderson Transition, *Phys. Rev. Lett.* **97**, 046803 (2006).
- [58] R. Dubertrand, I. García-Mata, B. Georgeot, O. Giraud, G. Lemarié, and J. Martin, Two Scenarios for Quantum Multifractality Breakdown, *Phys. Rev. Lett.* **112**, 234101 (2014).
- [59] H. Hiramoto and S. Abe, Dynamics of an electron in quasiperiodic systems. II. Harper's model, *J. Phys. Soc. Jpn.* **57**, 1365 (1988).
- [60] R. Ketzmerick, K. Kruse, S. Kraut, and T. Geisel, What Determines the Spreading of a Wave Packet?, *Phys. Rev. Lett.* **79**, 1959 (1997).
- [61] M. Larcher, F. Dalfovo, and M. Modugno, Effects of interaction on the diffusion of atomic matter waves in one-dimensional quasiperiodic potentials, *Phys. Rev. A* **80**, 053606 (2009).

- [62] Y. Wang, C. Cheng, X.-J. Liu, and D. Yu, Many-body critical phase: extended and nonthermal, Phys. Rev. Lett. **126**, 080602 (2021).
- [63] T. Xiao, D. Xie, Z. Dong, T. Chen, W. Yi, and B. Yan, Observation of topological phase with critical localization in a quasi-periodic lattice, Science Bull. **66**, 2175 (2021).
- [64] A. Pal and D. A. Huse, Many-body localization phase transition, Phys. Rev. B **82**, 174411 (2010).
- [65] R. Nandkishore and D. A. Huse, Many-body localization and thermalization in quantum statistical mechanics, Annu. Rev. Condens. Matter Phys. **6**, 15 (2015).
- [66] A. Avila, Global theory of one-frequency Schrödinger operators, Acta. Math. **1**, 215 (2015).
- [67] See Supplemental Material for details of the (i) Lyapunov exponent, (ii) larger κ case, (iii) finite size scaling, (iv) more perturbation results, (v) localization length and (vi) experimental realizations, which includes Ref. [66, 77, 80]
- [68] We particularly note that (i) The limit $\epsilon \rightarrow \infty$ is not a typo, but that γ_ϵ are actually a constant independent of ϵ , as shown by Avila's global theory and the asymptotic behavior of γ_ϵ in our model; (ii) The second equality is true because in our model, $T_i(\theta) = T_{i+\kappa}(\theta - 2\pi\alpha\kappa)$ and that \mathcal{T}_κ is independent of θ in the limit of $\epsilon \rightarrow \infty$ so that in that limit $\mathcal{T}_{m\kappa} = \mathcal{T}_\kappa^m$. See Supplementary Material [67] for more formal and detailed discussion.
- [69] A. Avila, S. Jitomirskaya, and C. A. Marx, Spectral Theory of Extended Harper's Model and a Question by Erdős and Szekeres, Invent. Math. **210**, 283 (2017).
- [70] Barry Simon and Thomas Spencer. Trace class perturbations and the absence of absolutely continuous spectra. Commun. Math. Phys. **125**: 113-125 (1989).
- [71] S. Jitomirskaya and C. A. Marx. Analytic quasi-periodic cocycles with singularities and the Lyapunov exponent of extended Harper's model. Commun. Math. Phys. **316**: 237-267 (2012).
- [72] See [70] or Proposition 7.1 in Ref. [71].
- [73] Here incommensurate distributions of zeros refers to that the hopping coefficients approach zero $t_{2j} \rightarrow 0$ on the lattice sites $2j$ which are incommensurately distributed over the whole system in the thermodynamic limit. To be more precise, the sequence $\{2j_k\}$ of sites with $t_{2j_k} \rightarrow 0$ is an infinite sequence which does not contain any infinite subsequence whose indices increase *linearly* over the system, or equivalently, it does not contain any infinite subsequence whose indices can match a sublattice of the whole system.
- [74] S. Iyer, V. Oganesyan, G. Refael, and D. A. Huse, Many-body localization in a quasiperiodic system, Phys. Rev. B **87**, 134202 (2013).
- [75] D. Barredo, S. de Léséleuc, V. Lienhard, T. Lahaye, and A. Browaeys, An atom-by-atom assembler of defect-free arbitrary two-dimensional atomic arrays, Science **354**, 1021 (2016).
- [76] M. Endres, H. Bernien, A. Keesling, H. Levine, E. R. Anschuetz, A. Krajenbrink, C. Senko, V. Vuletic, M. Greiner, and M. D. Lukin, Atom-by-atom assembly of defect-free one-dimensional cold atom arrays, Science **354**, 1024 (2016).
- [77] A. Browaeys and T. Lahaye, Many-body physics with individually controlled Rydberg atoms, Nat. Phys. **16**, 132 (2020).
- [78] S. de Léséleuc, V. Lienhard, P. Scholl, D. Barredo, S. Weber, N. Lang, H. P. Büchler, T. Lahaye, and A. Browaeys, Observation of a symmetry-protected topological phase of interacting bosons with Rydberg atoms, Science **365**, 775 (2019).
- [79] V. Lienhard, P. Scholl, S. Weber, D. Barredo, S. de Léséleuc, R. Bai, N. Lang, M. Fleischhauer, H. P. Büchler, T. Lahaye, and A. Browaeys, Realization of a Density-Dependent Peierls Phase in a Synthetic, Spin-Orbit Coupled Rydberg System, Phys. Rev. X **10**, 021031 (2020).
- [80] T.-H. Yang, B.-Z. Wang, X.-C. Zhou, and X.-J. Liu, Quantum Hall states for Rydberg arrays with laser-assisted dipole-dipole interactions, Phys. Rev. A **106**, L021101 (2022).
- [81] S. Ravets, H. Labuhn, D. Barredo, T. Lahaye, and A. Browaeys, Measurement of the angular dependence of the dipole-dipole interaction between two individual Rydberg atoms at a Förster resonance, Phys. Rev. A **92**, 020701(R) (2015).

Supplementary Material

This Supplemental Material provides additional information for the main text. In Sec. S-1, we give the details of computing Lyapunov exponent. The numerical results for larger κ are shown in Sec. S-2. In Sec. S-3, we study finite size scaling of mean fractal dimension of our model. In Sec. S-4, we present other forms of perturbation potentials and other values of λ in few-body calculations. In Sec. S-5, we give numerical results of localization length. Finally, we give details of experimental realization in Sec. S-6.

S-1. LYAPUNOV EXPONENT

In this section, we give a detailed derivation of Lyapunov exponent (LE) of the proposed model for arbitrary κ . We let $t_0 = 1$ for simplicity. For an irrational α , consider the quasiperiodic Schrödinger operators for the proposed model,

$$(H_{\lambda,\alpha,\theta}\psi)_n \equiv V_n\psi_n + t_n\psi_{n+1} + t_{n-1}^*\psi_{n-1}, \quad (\text{S1})$$

with

$$V_n(\theta) = \begin{cases} 2 \cos[2\pi(n-1)\alpha + \theta] & \text{for } n = 1 \bmod \kappa, \\ 2 \cos(2\pi n\alpha + \theta) & \text{for } n = 0 \bmod \kappa, \\ 0 & \text{otherwise,} \end{cases} \quad (\text{S2})$$

$$t_n(\theta) = \begin{cases} 2 \cos(2\pi n\alpha + \theta) & \text{for } n = 0 \bmod \kappa, \\ \lambda & \text{otherwise,} \end{cases} \quad (\text{S3})$$

$\theta \in [0, 2\pi)$ and $\lambda \neq 0$. Denote the m -step transfer matrix of the operator as $\mathcal{T}_{m_0+m, m_0}(\theta) \equiv T_{m_0+m-1}T_{m_0+m-2} \cdots T_{m_0+1}T_{m_0}$, where T_i is the one-step transfer matrix at site i satisfying

$$\begin{pmatrix} \psi_{i+1} \\ \psi_i \end{pmatrix} = T_i \begin{pmatrix} \psi_i \\ \psi_{i-1} \end{pmatrix} \quad (\text{S4})$$

and $T_i(\theta) = T_{i-\kappa}(\theta + 2\pi\kappa\alpha)$. The LE γ_0 of our proposed model can be computed through the complexified LE

$$\gamma_\epsilon(E) = \lim_{m \rightarrow \infty} \frac{1}{2\pi m} \int \ln \|\mathcal{T}_{m,1}(\theta + i\epsilon)\| d\theta, \quad (\text{S5})$$

where $\|A\|$ denotes the norm of the matrix A , i.e. the square root of the largest eigenvalue of $A^\dagger A$.

Observe that the κ -step transfer matrix can be written as

$$\begin{aligned} \mathcal{T}_{\kappa,1}(\theta + i\epsilon) &= \mathcal{T}_{2\kappa, \kappa+1}(\theta + i\epsilon - 2\pi\alpha\kappa) = \mathcal{T}_{3\kappa, 2\kappa+1}(\theta + i\epsilon - 4\pi\alpha\kappa) = \cdots \\ &= \frac{\begin{pmatrix} E/\lambda & -1 \\ 1 & 0 \end{pmatrix}^{\kappa-2}}{\lambda M(\theta + i\epsilon)} \begin{pmatrix} E - M(\theta + i\epsilon) & -M(\theta + i\epsilon) \\ \lambda & 0 \end{pmatrix} \begin{pmatrix} E - M(\theta + i\epsilon) & -\lambda \\ M(\theta + i\epsilon) & 0 \end{pmatrix} \\ &= \frac{1}{\lambda M} \begin{pmatrix} a_\kappa & -a_{\kappa-1} \\ a_{\kappa-1} & -a_{\kappa-2} \end{pmatrix} \begin{pmatrix} E^2 - 2EM & -\lambda E + \lambda M \\ \lambda E - \lambda M & -\lambda^2 \end{pmatrix}, \end{aligned}$$

where $a_\kappa = \Delta^{-1} [((\beta + \Delta)/2)^{\kappa-1} - ((\beta - \Delta)/2)^{\kappa-1}]$, $\Delta = \sqrt{\beta^2 - 4}$, $\beta = E/\lambda$ and $M(\theta + i\epsilon) = 2 \cos(\theta + i\epsilon)$. The basic point here is that $\mathcal{T}_{\kappa,1}$ is singular not analytic. While Avila's global theory is developed to one-frequency analytic cocycles [S1], here we will show how to extend it to deal with the singular setting.

We observe that $\mathcal{T}_{\kappa,1} \in SL(2, \mathbb{R})$, and it is singular only at $\epsilon = 0$, so that by Avila's global theory $\kappa\gamma_\epsilon$ is a convex, piecewise linear function with integer slopes for positive and negative ϵ separately, the main issue is the singular point $\epsilon = 0$. The key observation is to consider

$$\tilde{T}_\kappa(\theta) \equiv M(\theta)\mathcal{T}_{\kappa,1}(\theta) = \frac{1}{\lambda} \begin{pmatrix} a_\kappa & -a_{\kappa-1} \\ a_{\kappa-1} & -a_{\kappa-2} \end{pmatrix} \begin{pmatrix} E^2 - 2EM & -\lambda E + \lambda M \\ \lambda E - \lambda M & -\lambda^2 \end{pmatrix},$$

which are analytic about θ . Thus, the Lyapunov exponent of the new matrix is defined by

$$\tilde{\gamma}_\epsilon(E) := \lim_{m \rightarrow \infty} \frac{1}{2\pi m} \int \ln \|\tilde{\mathcal{T}}_m(\theta + i\epsilon)\| d\theta,$$

Meanwhile, by definition of Lyapunov exponent

$$\kappa\gamma_\epsilon(E) = \tilde{\gamma}_\epsilon(E) - \frac{1}{2\pi} \int_0^{2\pi} \ln |2 \cos(\theta + i\epsilon)| d\theta \quad (\text{S6})$$

where by classical Jenson's formula, one has

$$\int_0^{2\pi} \ln |2 \cos(\theta + i\epsilon)| d\theta = 2\pi|\epsilon|. \quad (\text{S7})$$

Since $\tilde{\mathcal{T}}_\kappa(\theta)$ is analytic, Avila's global theory [S1] ensures $\tilde{\gamma}_\epsilon(E)$ is a continuous, convex, piecewise linear function with respect to ϵ . By (S6) and (S7), one thus conclude $\kappa\gamma_\epsilon$ is a convex, continuous, piecewise linear function with integer slopes for any $\epsilon \in \mathbb{R}$.

In the following, we will show that $\gamma_0(E) = \gamma_\epsilon(E) = \gamma_\infty(E)$. Let us complexify the phase of \mathcal{T}_κ , and let ϵ go to $+\infty$,

$$\mathcal{T}_\kappa(\theta + i\epsilon) = \begin{pmatrix} a_\kappa & -a_{\kappa-1} \\ a_{\kappa-1} & -a_{\kappa-2} \end{pmatrix} \begin{pmatrix} -2\beta & 1 \\ -1 & 0 \end{pmatrix} + \mathcal{O}(e^{-\epsilon}) = \mathcal{T}'_\kappa + \mathcal{O}(e^{-\epsilon})$$

so that

$$\kappa\gamma_\epsilon(E) = \ln \|\mathcal{T}'_\kappa\| + \mathcal{O}(\epsilon^{-1}).$$

As we have proved, as a function of $\epsilon > 0$, $\kappa\gamma_\epsilon(E)$ is a convex, continuous, piecewise linear with integer slopes, which implies that, for all $\epsilon \in \mathbb{R}$

$$\gamma_\epsilon \equiv \frac{1}{\kappa} \ln \|\mathcal{T}'_\kappa\| = \frac{1}{\kappa} \ln \left| |a_{\kappa+1}| + \sqrt{a_{\kappa+1}^2 - 1} \right|.$$

In particular, $a_{1,2,3} = 0, 1, \beta$ respectively so that for $\kappa = 2$, the Lyapunov exponent

$$\gamma_0 = 1/2 \times \ln \left| (|E| + \sqrt{E^2 - \lambda^2}) / \lambda \right|$$

as discussed in the maintext.

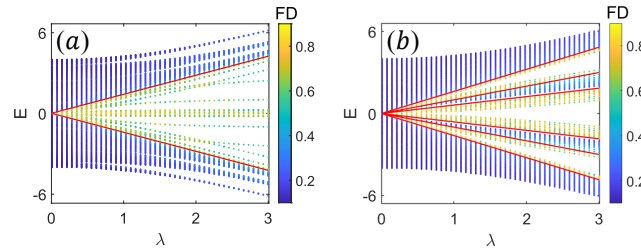


Figure S1. Fractal dimension (FD) of corresponding eigenstates as a function of energies E and constant hopping strength λ for (a) $\kappa = 3$ with lattice size $L = 987$ and (b) $\kappa = 4$ with lattice size $L = 2584$. The red lines denote the MEs given by analytic results, and t_0 is set to 1 as energy unit.

S-2. LARGER κ CASE

In the main text, we have shown the calculated mobility edges (MEs) for the case $\kappa = 2$. In this section, we present the analytic expression for the MEs with numerical verification for larger κ . The mobility edges occur at $a_{\kappa+1}^2 = 1$, which simplifies to $(\csc \phi \sin \kappa \phi)^2 = 1$, where $2 \cos \phi = \beta$. Therefore the MEs are at

$$E_c^{(\kappa)} = \pm 2\lambda \cos \frac{n_1 \pi}{\kappa - 1} \text{ or } \pm 2\lambda \cos \frac{n_2 \pi}{\kappa + 1}, \quad (\text{S8})$$

where $n_1 = 1, 2, \dots, \lfloor (\kappa - 2)/2 \rfloor$ and $n_2 = 1, 2, \dots, \lfloor \kappa/2 \rfloor$. In particular for the cases of $\kappa = 3$ or 4 , the MEs are given by

$$E_c^{(\kappa=3)} = \pm\sqrt{2}\lambda,$$

$$E_c^{(\kappa=4)} = \pm\lambda, \pm\frac{1+\sqrt{5}}{2}\lambda \text{ or } \pm\frac{1-\sqrt{5}}{2}\lambda.$$

As mentioned in main text, the FD tends to 1 and 0 for the extended and localized states, respectively, and $0 < \text{FD} < 1$ for critical states. Fig.S1 shows the fractal dimension (FD) as a function of λ for different eigenstates of energies E . The red lines represent the MEs for $\kappa = 3$ and $\kappa = 4$, respectively. The FD changes from 0 to value close to 0.5 when the energy and mark the localization-to-critical transition predicted by analytic results. Both two cases agree with the analytic expressions as expected.

S-3. FINITE SIZE SCALINGS

In this section, we study the finite size scaling of mean fractal dimension (MFD) of critical zone and localized zone. We choose $\kappa = 2$ case as an example. MFD of critical zone is the averaged fractal dimension of all eigenstates in critical regime, i.e., eigenstates with energies $|E| < |\lambda|$. MFD of localized zone can be obtained in a similar way. Fig. S2 (a) and (b) show the MFD as a function of $1/n$ for the critical zone and localized zone, respectively. It is observed that MFD approaches to finite value between 0 and 1 for the critical zone, and approaches to 0 for the localized zone.

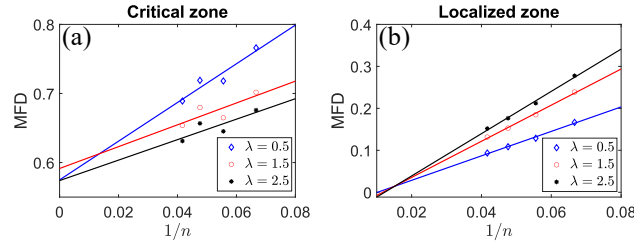


Figure S2. MFD as a function of $1/n$ for the (a) critical zone and (b) localized zone with different λ . Here n is the index of Fibonacci numbers F_n .

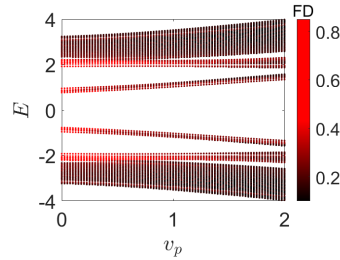


Figure S3. Fractal dimension (FD) of different eigenstates as a function of corresponding energies E and perturbative on-site potential v_p . with $m = 1$, $\lambda = 2.0$, $t_0 = 1.0$ and $L = 2584$.

S-4. MORE PERTURBATION RESULTS

In the main text, we have showed that the critical zone is robust against experimentally relevant onsite perturbation and is also against interactions between particles. To further demonstrate robust critical zone is indeed protected by zeros of hopping coefficients, we present more numerical results of perturbations. In this section, the on-site perturbation V_p is given by

$$V_p = v_p \sum_j \cos(2\pi m \alpha j + \phi) n_j, \quad (\text{S9})$$

with $m \in \mathbb{Z}$, and the hopping perturbation T_p is given by

$$T_p = t_p \sum_j [\cos(2\pi m \alpha j + \phi) b_j^\dagger b_{j+1} + \text{H.c.}], \quad (\text{S10})$$

A. Simplest onsite perturbation

We first consider the onsite perturbation V_p with $m = 1$. Fig. S3 shows FD of eigenstates as a function of energies E and strength of perturbations v_p . The critical zone persists for a range of perturbation v_p . As v_p increases, the critical zone shrinks since the on-site perturbation localizes some of the critical states. When v_p is large enough, all the critical states will be localized as expected. This result is consistent with the experiment-relevant perturbation in the main text.

B. More perturbations

Moreover, we choose $m = 3$ and consider both onsite perturbation and perturbative hopping term. Fig. S4 shows FD of eigenstates as a function of energies E and strength of perturbations and interactions. Similar to the results in the main text and last subsection, the critical zone is robust against moderate perturbation and can persist for a range of t_p or v_p as expected. Furthermore, it is observed that adding perturbative hopping term T_p is easier to drive system into localized phase compared to adding perturbative on-site term V_p . This is because T_p directly acts on the hopping terms and is easier to remove the zeros of hopping coefficients compared to the on-site perturbation V_p . Another feature is that a second ME emerges due to perturbations, and the localization transitions start from center of the spectrum instead of edge of the spectrum. One can introduce more terms as perturbation and choose m as arbitrary integer and will obtain similar results, indicating robustness of the MEs protected by the generic mechanism.

We also present more numerical results of robustness against interactions. For the case $\lambda = 2$, $t_0 = 1$ and $V = 1.4$, the critical energy is less prominent compared with the results in the main text, but the relation $E_{c,l} = (c\lambda + lE_{\max})$ still holds and single particle ME still exists as illustrated in Fig. S4(b).

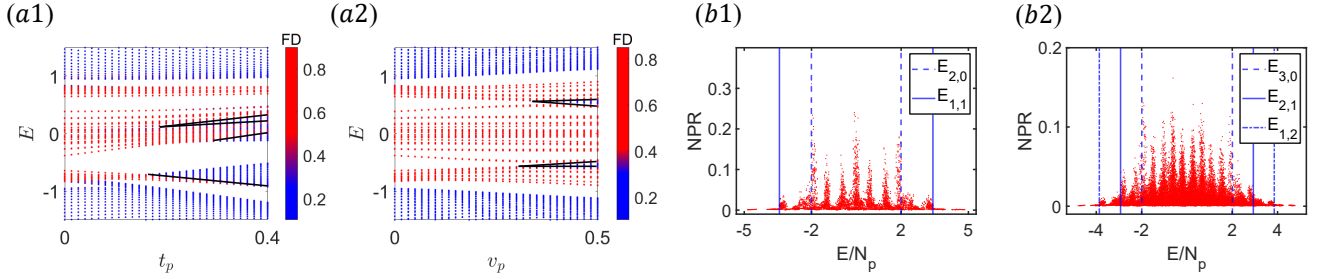


Figure S4. Fractal dimension (FD) of different eigenstates as a function of corresponding energies E and (a1) strength of perturbative hopping term t_p and (a2) perturbative on-site potential v_p . New MEs are marked by black lines. Other parameters are $\lambda = 0.8$ and $L = 2584$. And Normalized participation ratio (NPR) as a function of energy density E/N_p of few hardcore bosons case with nearest neighbor interaction $U = 1.4$, with $\lambda = 2.0$, $t_0 = 1.0$ and (b1) $N_p = 2$, $L = 120$ (b2) $N_p = 3$, $L = 60$. The critical energy $E_{2,0}$ ($E_{3,0}$) is equal to the single particle ME $E = \lambda$ for two (three) bosons case.

S-5. LOCALIZATION LENGTH

In this section, we numerically verify the localization length ξ obtained in the main text. As shown in Fig. S5, the red lines represent $|\psi|_{\max} \exp(-|i - i_0|/\xi)$, where $|\psi|_{\max}$ is the maximum values of $|\psi|$ in the two peaks, i_0 is the corresponding lattice sites and ξ is the localization length which is given by $\xi(E) = 2/\ln[(|E| + \sqrt{E^2 - \lambda^2})/|\lambda|]$. It is indicated the analytic expressions of the localization length ξ well describe the localization features of the corresponding eigenstates.

S-6. EXPERIMENTAL REALIZATION

In this section, we illustrate how to realize the lattice model in the main text. Our basic idea is to use well-tuned Rydberg atoms to simulate hard-core bosons with hoppings and on-site potentials controlled by external fields. We shall realize the Hamiltonian

$$H = \sum_{j_x} (J_{j_x} \sigma_{j_x,A}^+ \sigma_{j_x,B}^- + \lambda \sigma_{j_x,A}^+ \sigma_{j_x+1,B}^- + \text{H.c.}) + \frac{1}{2} \sum_{j_x, s=\{A,B\}} V_{j_x} (\mathbb{1} + \sigma_{j_x,s}^z), \quad (\text{S11})$$

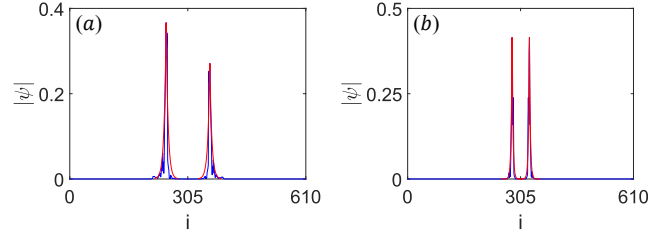


Figure S5. Spatial distributions of eigenstates. Blue lines represent $|\psi|$, where ψ is the eigenstates corresponding to (a) $E = -2.1(6)t_0$ with $\lambda = 2t_0$, (b) $E = -1.3(5)t_0$ with $\lambda = t_0$. Here we fix $L = 610$. The red lines represent $|\psi|_{\max} \exp(-|i - i_0|/\xi)$.

which can be transformed into the model in the main text by relabeling site index $j_x \rightarrow 2j - 1$ for j_x on A-leg and $j_x \rightarrow 2j$ for j_x on B-leg, and defining bosonic operator $b_j^\dagger = |1\rangle_j \langle 0|_j$ at each site, with $|1\rangle \equiv |\uparrow\rangle$ and $|0\rangle \equiv |\downarrow\rangle$. In the following we shall take ^{87}Rb atoms as an example. For ^{87}Rb , two Rydberg states are chosen to simulate spin 1/2 at each site with $|\downarrow\rangle \equiv |70, S\rangle$ and $|\uparrow\rangle \equiv |70, P\rangle$. We consider the two-leg superarray of Rydberg atoms, with each trapped in optical tweezers. We consider the two-leg superarray of Rydberg atoms, with each trapped in optical tweezers. An effective Zeeman splitting $M_{j_x,s}$ is introduced along the x direction, with $M_{j_x+1,s} - M_{j_x,s} = \Delta$, $M_{j_x=0,A} = 0$ and $M_{j_x=0,B} = 0$. Three Raman beams are applied to generate Raman and AC Stark potential. The total Hamiltonian of the system is given by,

$$H = H_{\text{dipole}} + H_{\text{Zeeman}} + V_R(\mathbf{r}, t) + V_{\text{AC}}(\mathbf{r}), \quad (\text{S12})$$

which includes the bare dipole-dipole interactions [S2]

$$H_{\text{dipole}} = \sum_{j_x} J_y^0 \sigma_{j_x,A}^+ \sigma_{j_x,B}^- + J_d^0 \sigma_{j_x-1,A}^+ \sigma_{j_x,B}^- + \sum_{|i-j|>1} \frac{J_{ij}}{R_{ij}^3} \sigma_{i,A}^+ \sigma_{j,B}^- + \text{H.c.},$$

with $J_y^0 = C_3/a_y^3$ and $J_d^0 = C_3/(a_x^3 + a_y^3)^{3/2}$, the effective Zeeman energy gradient term,

$$H_{\text{Zeeman}} = \frac{1}{2} \sum_{j_x, s=\{A,B\}} M_{j_x,s} \sigma_{j_x,s}^z,$$

the Raman coupling potential obtain from time-dependent perturbation [S3]

$$V_R(\mathbf{r}, t) = \frac{\Omega_1(\mathbf{r}, t)^* \Omega_2(\mathbf{r}, t)}{\Delta_i} \sigma_{j_x, j_y}^x,$$

and the AC Stark term

$$V_{\text{AC}}(\mathbf{r}) = \frac{|\Omega_3(\mathbf{r})|^2}{\Delta'_i}.$$

As discussed in the main text, the bare dipole-dipole interactions between Rydberg states with the same Zeeman energy constitute the constant hopping coupling $\lambda = J_d^0$. In the following, we discuss the scheme for realizing the incommensurate hopping couplings and on-site potential.

A. The incommensurate hoppings

The incommensurate hoppings are simulated by laser-assisted dipole-dipole interactions. The bare dipole-dipole interactions between legs on the same j_x are suppressed by the large Zeeman splitting Δ , but can be further restored by applying the Raman coupling potential V_R . The Raman coupling potential is generated by two Raman lights with Rabi-frequencies $\Omega_{1,2}$ and the frequencies $\omega_{1,2}$. When the frequency difference satisfies nearly resonant condition $\omega_1 - \omega_2 \approx \Delta$, then the Zeeman detuning Δ is compensated by the two-photon process. Here we choose $\Omega_1 = \Omega_0 \cos(2\pi\alpha j_x + \frac{\pi}{4})e^{i\theta_1}$ and $\Omega_2 = \Omega_0 \sin(2\pi\alpha j_x + \pi j_y + \frac{\pi}{4})e^{i\theta_2}$, direct calculation yields the Raman potential

$$V_R(\mathbf{r}, t) = \sum_{j_x, j_y} \frac{|\Omega_0|^2}{2\Delta_i} \cos(4\pi\alpha j_x) \cos(\pi j_y) e^{i\delta\theta} \sigma_{j_x, j_y}^x + \text{H.c.}, \quad (\text{S13})$$

with $\delta\theta = \theta_2 - \theta_1$. So we choose $\theta_2 = \theta_1 + n\pi$, which can be realized in experiment. To the lowest order, the effective exchange couplings are [S3]

$$J_{j_x} = \frac{|\Omega_0|^2}{\Delta\Delta_i} \cos(2\pi\alpha j_x) J_y^0, \quad (\text{S14})$$

which realize the incommensurate hopping coefficients. Notice that the transition between j_x and $j_x + 2$ and longer distance are suppressed by larger Zeeman energy offset (i.e., at least 2Δ) and cannot be induced by two-photon process. To prohibit laser-assisted exchange coupling within the same leg, we use the angular dependence of dipole-dipole interaction $J = d^2(3\cos^2\theta_{ij} - 1)/R_{ij}^3$ as discussed in the main text. We arrange the Rydberg atoms along the "magic angle" $\theta_m = \arccos(1/\sqrt{3}) \approx 54.7^\circ$, at which the dipolar interactions vanish. So there is no hopping coupling generated by Raman potential along the x direction.

B. The incommensurate on-site potential

We apply another standing wave field to generate an incommensurate on-site potential $V_{AC}(\mathbf{r})$, which is $\Omega_3(\mathbf{r}) = \Omega'_0 \cos(2\pi\alpha j_x)$. Together with an additionally correction from Raman potential, the total on-site term is given by

$$\begin{aligned} V_{\text{on-site}} &= \frac{|\Omega_1|^2 + |\Omega_2|^2}{\Delta_i} + V_{AC} \\ &= \frac{1}{\Delta_i} \left[|\Omega_0|^2 \cos^2(2\pi\alpha j_x + \frac{\pi}{4}) + |\Omega_0|^2 \sin^2(2\pi\alpha j_x + \pi j_y + \frac{\pi}{4}) \right] + \frac{1}{\Delta'_i} [|\Omega'_0|^2 \cos^2(2\pi\alpha j_x)] \\ &= \frac{|\Omega_0|^2}{\Delta_i} + \frac{|\Omega'_0|^2}{2\Delta'_i} + \frac{|\Omega'_0|^2}{2\Delta'_i} \cos(4\pi\alpha j_x), \end{aligned} \quad (\text{S15})$$

of which the constant part can be neglected and we can reach the desired on-site incommensurate potential.

C. Experimental parameters

Here, we also give an estimate of the orders of magnitude of the relevant experimental parameters. The data given here are based on ^{87}Rb atoms. For the states $|70S\rangle$ and $|70P\rangle$, $C_3 = 4196\text{MHz} \cdot \mu\text{m}^{-3}$. Then with $a_y/a_x = 0.8$, $|\Omega_0| = |\Omega'_0| = 200\text{MHz}$, $\Delta = 10\text{MHz}$ and $\Delta_i = 16.5\text{GHz}$ and $a_x = 12.5\mu\text{m}$, we obtain the model with $t_0 = |\Omega_1\Omega_2 J_y^0 / (2\Delta\Delta_i)| = 0.5\text{MHz}$, $\lambda = 1\text{MHz}$

To observe the correlated effects, the lifetime of the system should be large compared to the characteristic time of the system. For $\lambda = 1\text{MHz}$, a lifetime of at least $\tau > \tau_0 = 100J_0^{-1} = 100\mu\text{s}$ is needed. The lifetime of the Rydberg states $|70S\rangle$ and $|70P\rangle$ are $370\mu\text{s}$ and $750\mu\text{s}$ respectively. The lifetime of $6P$ states, which the Raman process coupled, has a lifetime of $\tau_{6P} = 130\text{ns}$. So for the single photon detuning $\Delta_i = 16.5\text{GHz}$ and $\Delta'_i = 20\text{GHz}$, the lifetime can be estimated by $\tau = (2|\Omega_0|/\Delta_i + |\Omega'_0|/\Delta'_i)^{-2} \tau_{6P} \approx 110\mu\text{s} > \tau_0$.

* These authors contribute equally to this work.

† qizhou@nankai.edu.cn

‡ xiongjunliu@pku.edu.cn

[S1] A. Avila, Global theory of one-frequency Schrödinger operators. *Acta. Math.* **1**, 215 (2015).

[S2] A. Browaeys and T. Lahaye, Many-body physics with individually controlled Rydberg atoms, *Nat. Phys.* **16**, 132 (2020).

[S3] T.-H. Yang, B.-Z. Wang, X.-C. Zhou, and X.-J. Liu, Quantum Hall states for Rydberg arrays with laser-assisted dipole-dipole interactions, *Phys. Rev. A* **106**, L021101